Breakdown of kinetic compensation effect in physical desorption

Nayeli Zuniga-Hansen, Leonardo E. Silbert, and M. Mercedes Calbi

Phys. Rev. E **98**, 032128 — Published 24 September 2018

DOI: 10.1103/PhysRevE.98.032128

Breakdown of Kinetic Compensation Effect in Physical Desorption

Nayeli Zuniga-Hansen*
Department of Physics & Astronomy, Louisiana State University, Baton Rouge, Louisiana 70803, U.S.A.

Leonardo E. Silbert
School of Math, Science and Engineering, Central New Mexico Community College, Albuquerque, New Mexico 87106, U.S.A.

M. Mercedes Calbi
Department of Physics, University of Denver, Denver, Colorado 80208, U.S.A.
(Dated: August 16, 2018)

The kinetic compensation effect, observed in many fields of science, is the systematic variation in the apparent magnitudes of the Arrhenius parameters, the activation energy E_a and the preexponential factor ν, as a response to perturbations. If, in a series of closely related activated processes, these parameters exhibit a strong linear correlation, then it is expected that an isokinetic relation will occur, and the rates assume a common value at the compensation temperature T_c. The reality of these two phenomena continues to be debated as they have not been explicitly demonstrated and their physical origins remain poorly understood. Using kinetic Monte Carlo simulations on a model interface, we explore how site and adsorbate interactions influence the Arrhenius parameters during a typical desorption process. We find that their transient variations result only in a partial compensation as the variations in the prefactor are not large enough to completely offset those in E_a. In addition, the observed isokinetic relation arises as a result of a transition to a non-interacting regime, and not due to compensation between E_a and $\ln\nu$. These results provide a deeper insight into the microscopic events from which compensation effects and isokinetic relations originate in this system, suggesting similar mechanisms may be at play in other systems where compensation effects have been reported.

PACS numbers: PACS numbers: 82.20.Db, 68.43.Vx, 68.43.Nr, 68.43.De

I. INTRODUCTION

Many physical, biological, and chemical processes exhibit a strong temperature dependence, in the sense that they rely on thermally activated mechanisms to overcome energy barriers in order for the process to proceed. The rate k of many such processes follows an Arrhenius type behavior

$$k = \nu \exp\left(\frac{-E_a}{k_B T}\right), \tag{1}$$

where E_a is the activation energy, ν the preexponential factor, T the temperature, and k_B is Boltzmann's constant. When a series of measured values of $\ln k$ is plotted as function of $1/T$ in a so-called Arrhenius plot, the activation energy is extracted from the slope, and the preeponential factor from the $y-$intercept [1].

A characteristic feature in a series of closely related thermally activated processes where a parameter has been varied (e.g., the concentration of an additive in a chemical reaction) is a systematic change in the apparent magnitudes of E_a and ν [2–4] as a response to perturbations, known as the *kinetic compensation effect* (KCE). A series of experiments carried out in this fashion usually yields a set of Arrhenius plots with different slopes [5, 6] that intersect at a common *compensation temperature* T_c [2, 4, 5, 7], such as the hypothetical set schematically represented in Fig. 1.

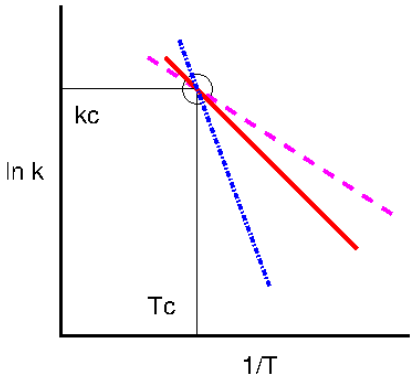

FIG. 1: (Color Online) Schematic idealized Arrhenius plots for a set of closely related thermally activated processes. The $\ln k = \ln\nu - {}^{E_a}/_{k_B T}$ curves cross at the compensation temperature T_c, where the rates appear to have the same value, k_c.

With the extracted Arrhenius parameters from each activated process, one can construct a Constable plot [8], $\ln\nu_i$ vs. $E_{a,i}$ [2, 9, 10], such as that schematically represented in Fig. 2. The subindex i indicates that the data pair was extracted from the i^{th} Arrhenius curve in the set. Following this method of analysis, a kinetic compensation effect is observed when the data points on the

* zunigahansen@lsu.edu

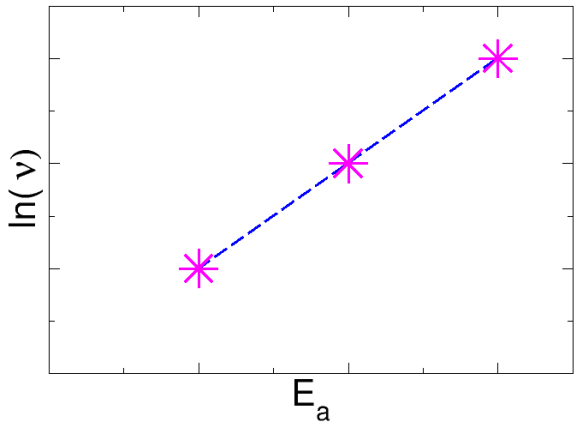

FIG. 2: (Color Online) A schematic idealized Constable plot for a set of closely related thermally activated processes. Each data point represents a data pair of *apparent* Arrhenius parameters $[E_{a,i}, \ln \nu_i]$ extracted from the slope and $y-$intercept, respectively, of the corresponding i^{th} plot in Fig. 1.

Constable plot fall on a straight line [7], and satisfy the linear relationship [5, 6]

$$\ln \nu_i = \beta E_{a,i} + \alpha, \tag{2}$$

where α and β are constants.

Historically, the KCE has been defined interchangeably with the isokinetic relation (IKR) [11], defined as $\beta = \frac{1}{k_B T_c}$ [4, 7]. This is because the observation of one phenomenon is thought to directly imply the occurrence of the other [2, 11]. In Fig. 1 the IKR is the point where the Arrhenius plots cross at T_c, where the rates "become the same and independent of external parameters and perturbations" [2, 5, 7, 12, 13]. If both the KCE (Eq. 2) and the IKR are satisfied, then it is expected that one can combine Eq. 1 with Eq. 2, $ln\nu_i = \ln k_i + \frac{E_{a,i}}{k_B T} = \beta E_{a,i} + \alpha$ and, equating coefficients, obtain the slope $\beta = {}^1/_{k_B T_c}$, and the $y-$intercept $\alpha = \ln k_c$, where k_c is the rate of all processes at T_c [2, 4, 5, 9].

Liu and Guo note [2] that this is only exact when the linear correlation coefficient between data points in the Constable plot is 1. In addition, they propose that the KCE and IKR are separate phenomena, which may be observed independently and should be characterized as such. The KCE should be identified solely by the strong linear correlation between E_a and $\ln \nu$ [2, 6, 7, 9, 13, 14], and the IKR by the convergence of Arrhenius plots around a single temperature [2, 13].

The extraction of parameters from the slope and $y-$intercept of an Arrhenius plot has proven to be a useful and important method that allows for the semi-empirical determination of rates [11, 15]. However, it has been widely accepted that E_a and ν need not be constant throughout many activated processes [6, 16–21]. The current physical explanation for the KCE establishes that the changes in E_a must be 'compensated' by a concomitant change in ν, in the same direction and with nearly the same magnitude, such that the overall rate remains relatively unchanged [2–4, 10, 12, 17, 21–24], and therefore the different values of E_a and $\ln \nu$ satisfy Eq. 2 for constant α and β. If true, this may justify the extraction of fixed values from the Arrhenius plots. However, this behavior has not been explicitly demonstrated [1, 2, 25], but has been the *a priori* assumption behind many studies that attempt to characterize the transient variations in E_a and ν [2, 3, 7, 10, 22, 23] through analytical expressions.

The proposed strong interdependence between E_a and $\ln \nu$ has been attributed to them being obtained from the same temperature dependent data [2, 7, 26], instead of through independent measurements (which are not always possible). This could be, as mentioned by Cornish-Bowden in [26], the consequence of the two parameters being "largely the same variable looked at in two ways".

Moreover, some instances of the IKR do not yield a compensation temperature that falls within the experimental range, and is therefore found by extrapolation [4, 26]. Thus the reality of the KCE and the IKR continue to be the subject of heated debate, as they are often believed to have a purely mathematical origin [7, 9, 15, 26, 27], or to be the consequence of experimental errors [7], and to lack any physical or chemical significance.

Nevertheless, the KCE and IKR, as well as the closely related enthalpy-entropy compensation, continue to be reported in many different areas of science, such as temperature programmed desorption [1], fouling [15], grain boundary migration [10], heterogeneous catalysis [3], crystallization of amorphous solids [28], glass transitions [29], adsorption [5, 30, 31], chemical reactions [5], molecular self-assembly [12, 32], and the melting of solids [24] among others.

As previosuly stated, much of the existing work is centered around the derivation of analytical expressions for E_a and ν [1, 22, 23], where a relation between the parameters is assumed, such that if one varies, the other varies, by an equal or nearly equal amount. The net effect is expected to be the compensation effect that leaves the rate relatively unchanged [1–3, 22, 23, 33, 34]. Although most authors agree that there is no general rule that dictates the occurrence of this mutually offsetting behavior [24, 33, 34], the strong linear correlation is cited as experimental evidence for it.

In the present work we follow the reverse approach, through the *ab initio* kinetic Monte Carlo [35] calculation of the variations in the activation energy as function of the decreasing coverage during the thermal desorption of interacting and non-interacting adsorbates from an energetically homogeneous, crystalline lattice. The numerical results also allow us to extract the preexponential factor, and therefore to verify and explicitly quantify the level

of compensation that has not been successfully achieved to date using more traditional methods.

This approach falls in line with the idea proposed by Liu and Guo in [2], where they mention the need for a study that captures the events at the molecular level, and without using preconceived functional forms. To our knowledge, this has not been done before.

Our numerical results span a range of adsorbate-adsorbate attractive interaction strengths, calculated as a percentage of the fixed surface binding energy. This provides the experimental parameter to be altered in a series of similar activated processes while keeping the substrate structure fixed.

II. MODEL SYSTEM AND METHODOLOGY

Temperature programmed desorption (TPD), or thermal desorption spectroscopy, is an experimental technique used in surface science to extract surface parameters such as binding energies, pore distribution [36], and sorption capacity, and it has applications in chemical speciation [37] and contaminant removal [38]. In a typical experiment, a surface in an evacuated chamber is exposed to a gas until the desired uptake is achieved. The sample is then heated with a linear temperature ramp of the form $T(t) = T(0) + \gamma t$, where γ is the size of the temperature step, and t is time. Experimental results are in the form of a peak in the rate of desorption $\dot{\theta}(T)$ as a function of the increasing temperature T [39].

The most common method of data analysis starts with the Polanyi-Wigner equation, given by

$$\dot{\theta} = \theta^n \nu e^{-E_a/k_B T}, \tag{3}$$

where θ is the fractional surface coverage, and n is the order of the process. Physical desorption from a uniform planar surface corresponds to order 1, thus we set $n = 1$ for the remainder of the present work. In the corresponding Arrhenius plot the rate is calculated as $k \equiv \dot{\theta}/\theta$. The parameters of interest, E_a and $\ln \nu$, can be extracted from the slope and $y-$intercept, respectively. As discussed before, such a parameterization has proven useful in the semi-empirical determination of rates [15]. However, the parameters E_a and ν may exhibit variations throughout the desorption process due to one or more factors, such as surface energetic heterogeneity [40, 41], lateral interactions [1, 25], multiple chemical species [42], and/or changes in surface configuration [22].

Our methodology was to simulate a TPD process from a quasi-two dimensional, square lattice of side L, with $N = L^2 = 1600$ sites and periodic boundary conditions using a kinetic Monte Carlo algorithm [35]. The lattice is energetically homogeneous, so that the j^{th} site has a binding energy $E_{jb} = E_b = 100$ in units where $k_B = 1$. We explore attractive interaction strengths ϵ in the range from $0 \leq \epsilon \leq 0.9E_b$. To track the desorption process, the kinetic Monte Carlo scheme follows a series of steps. First, the initial conditions are specified, including the binding and interaction energies, initial temperature (which is altered depending on ϵ), step size, and initial surface coverage (which is set to 100% in all cases). The second step is to calculate the number of occupied nearest neighbors per site and the site energies. Next, the probabilities associated with each of the allowed transitions are calculated as $W_j = e^{\beta E_j}$, where E_j is the energy barrier of the j^{th} adsorption site, calculated as

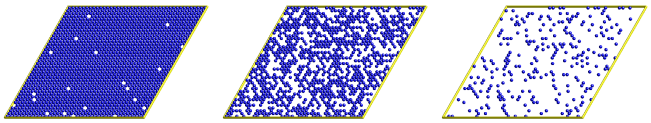

FIG. 3: (Color Online) Visualization of the kinetic Monte Carlo simulations during a desorption run for a 2D square lattice substrate. The snapshots are in order of increasing temperature, from left to right; blue (filled) circles represent occupied sites ($E_b = 100$, $\epsilon = 0$).

$$E_j = E_b + \sum_{m=1}^{z} n_{jm}\epsilon, \tag{4}$$

where each site j picks up an energy contribution from its m nearest occupied neighbors. Thus, $n_{jm} = 1$ when a neighbor site is occupied, and is zero if empty. Next, an allowable transition - desorption or diffusion to a neighboring site - is selected by generating a random number x_1 between 0 and 1. The change of state that takes place is the one with the largest probability, which satisfies the following inequality

$$\frac{1}{W}\sum_{i=1}^{k-1} W_{ji} < x_1 < \frac{1}{W}\sum_{i=1}^{k} W_{ji}, \tag{5}$$

where $W_{ji} = e^{\beta(E_j - E_i)}$ is the transition probability from state j to state i. The sum is over all k allowed transitions for a particle in site j, and W is the sum of all probabilities. Lower probability transitions are still allowed so that the system evolves in a free manner, rather than forcing it through a particular path. After every change of state, the time variable increases by a fractional amount determined by a second random number. The temperature is increased as $T = T_o + \gamma t$, where a change occurs only when γt is incremented by 1. The average site occupancy and energy are recorded at every iteration, and the process is repeated until the lattice is completely empty. The results are obtained as an (ensemble) average over many independent runs. The resultant coverage decrease curve can be fitted using a Fermi-Dirac distribution function

$$\theta = \frac{1}{1 + e^{\beta(\varepsilon - \mu)}}, \tag{6}$$

where the chemical potential μ can be extracted for every data point using the calculated average site occupancy and energy. Snapshots of the computer simulations are shown in Fig. 3.

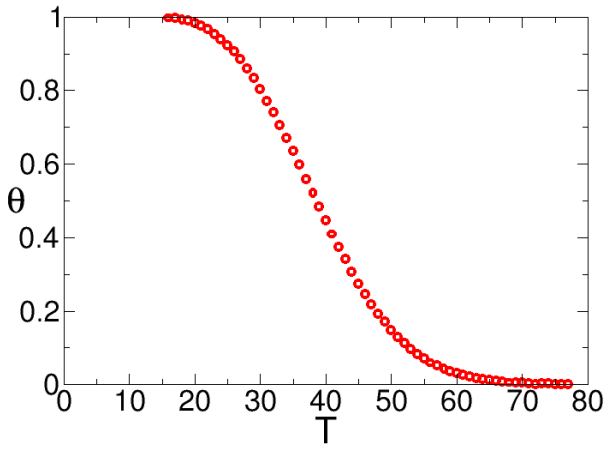

FIG. 4: (Color Online) Typical profile for the numerical simulation of the thermal desorption of non-interacting adsorbates from a 2D square lattice starting from full fractional coverage ($\theta = 1$). As the temperature (T) increases the coverage (θ) decreases. The site binding energy is set to $E_b = 100$ and the interaction energy is set to $\epsilon = 0$ (in simulation units).

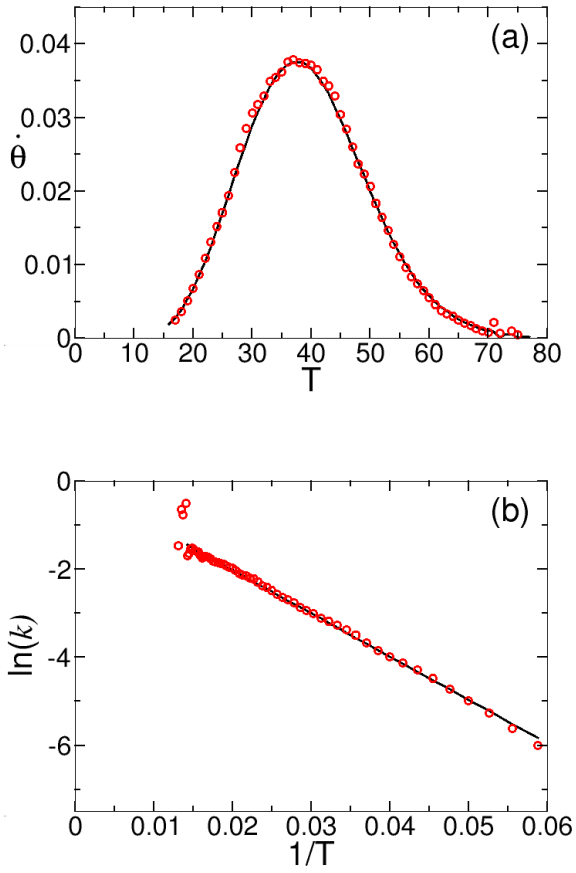

FIG. 5: (Color Online) Rate of coverage decrease ($\dot{\theta}$) as a function of temperature (T) (Fig. (a)), and corresponding Arrhenius plot (Fig. (b)) for the thermal desorption of non-interacting species ($\epsilon = 0$) from a square lattice with binding energy $E_b = 100$. The solid lines in Fig. (a) represent the fit to Eq. 3, and to the Arrhenius plot in Fig. (b), $\ln k = -\beta E_a + \ln \nu$, with $k \equiv \dot{\theta}/\theta$. Scatter in the numerical data at higher temperatures in the Arrhenius plot is due to division by small numbers as the surface coverage reaches zero.

III. RESULTS

The simulation results are in the form of the substrate fractional coverage $\theta(T)$ as function of increasing temperature T. A typical simulation data set is shown in Fig. 4 for the non-interacting species examples shown in Fig. 3. The corresponding rate and Arrhenius plots are shown in Fig. 5.

The first step is to verify that the simulation results in the non-interacting regime ($\epsilon = 0$) can be fitted to Eq. 3. This is shown in Fig. 5(a) where the numerical derivative $\dot{\theta}$ (symbols) is superimposed with the analytically calculated rate (solid lines) using Eq. 3, for fixed $E_a = 100$, and $\nu = 1$, and the coverage decrease data θ. Also in Fig. 5(b) is a linear fit to the corresponding Arrhenius plot, from which the following parameters were extracted: $E_a = 100 \pm 2$ and $\nu = 1 \pm 0.01$ (extrapolated $y-$intercept). The value for E_a, as expected, matches the input binding energy, E_b, within error.

A. Activation Energy

The average site occupancy data are plotted as a function of temperature in Fig. 6(a), and the corresponding Arrhenius curves are plotted as a function of $\frac{1}{T}$ in Fig. 6(b). The average activation energy per site is plotted in Fig. 7 as function of coverage (symbols). These results correspond to various regimes of interaction strength, as indicated in the figure legends. In the non-interacting regime, the activation energy remains constant and matches the binding energy, as expected, which is consistent with the fact that it represents the only energetic barrier to desorption. This feature of the non-interacting regime also applies locally at each site. In the case of interacting species, on the other hand, additional contributions from site-occupied nearest neighbors result in a stronger binding of the adsorbates to the surface, which varies locally due to the heterogeneous distribution of interacting occupied sites throughout the desorption process. This leads to an enhanced effective desorption barrier, and also to an increasing curvature of the Arrhenius plots as function of increasing ϵ. The increased effective potential barrier results in the reduced motility of the particles on the surface due to cluster for-

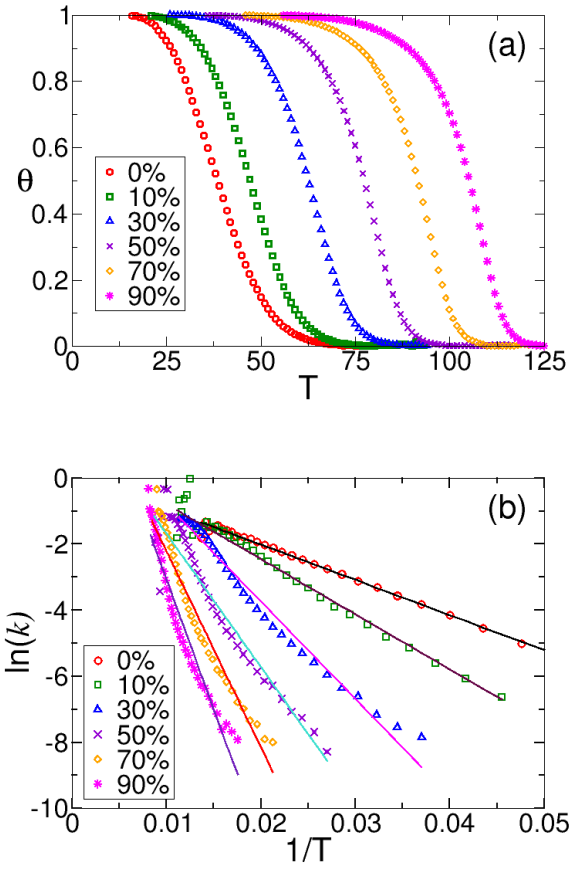

FIG. 6: (Color Online) Fractional coverage decrease data as function of temperature (Fig. (a)) for all regimes of interaction strength, indicated in the legend as a percentage of the surface binding strength $E_b = 100$. Corresponding Arrhenius plots (Fig. (b)) ($\ln \dot{\theta}/\theta$ vs.$^1/_T$) shown with the corresponding best linear fit (solid lines). The curvature of the plots increases with interaction strength.

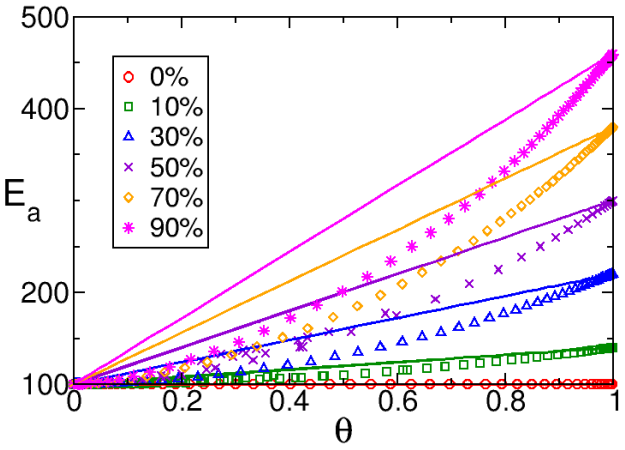

FIG. 7: (Color Online) Magnitude of the activation energy E_a as a function of coverage θ (symbols) for different interaction strengths, indicated in the legend as a percentage of the surface binding strength $E_b = 100$. The solid lines are a mean field (MF) analysis of the data.

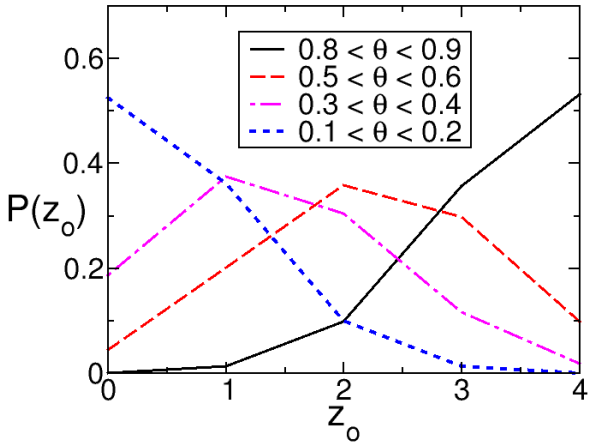

FIG. 8: (Color Online) Distributions $P(z_o)$ of the interacting site-occupied coordination number z_o at several values of the coverage θ (indicated in the legend). For this representative example $\epsilon = 30\%$. Other non-zero interaction energies exhibit similar behavior.

mation, and this decreased freedom to diffuse and desorb, combined with energetic heterogeneity, leads to a more pronounced curvature [44].

In a mean field (MF) approximation, the additional contributions to the activation energy due to occupied sites interacting with occupied neighbors is given by $z\theta\epsilon$, where z is the coordination number of the (square) lattice (here $z = 4$), and ϵ is the adsorbate-adsorbate interaction energy. The total mean activation energy is $< E_a >= (1 + zf\theta)E_b$, where $f = \epsilon/E_b$ is the fractional interaction energy. This analysis is shown by the solid lines in Fig. 7, where it can be seen that the MF approach is only accurate for the non-interacting regime (when $f = 0$), and for interacting systems at extreme coverage values (i.e. when $\theta = 1$ and 0). The reason behind this is that the MF approach presupposes that, at the molecular level, each site sees the same number of occupied neighbors throughout the substrate. In other words, the coordination of occupied interacting sites z_o is delta-function distributed. This is only true at complete coverage, where the distribution of interacting sites is $P(z_o) = \delta(z_o - 4)$, and again at zero coverage, where $P(z_o) = \delta(0)$. Thus, deviations from the MF picture originate from the distribution of interacting sites during the

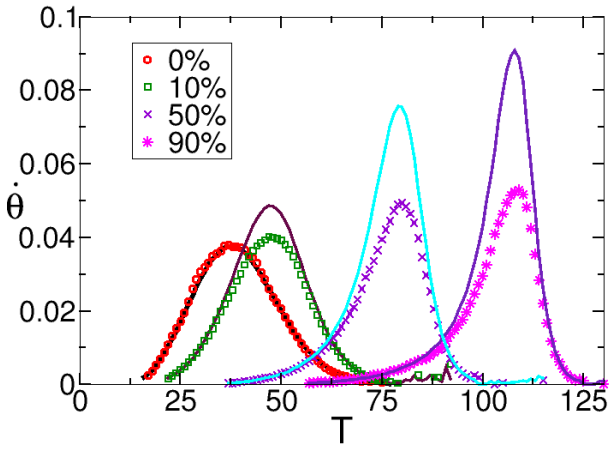

FIG. 9: (Color Online) Rate of coverage decrease ($\dot{\theta}$) computed as the numerical time-derivative of the coverage decrease data (symbols) from Fig. 6(a) for selected regimes of interaction strength, indicated in the legend as a percentage of the surface binding strength $E_b = 100$. These are compared to the analytically calculated rates (solid lines), using Eq. 3 with $\nu = 1$, and the numerical data for E_a.

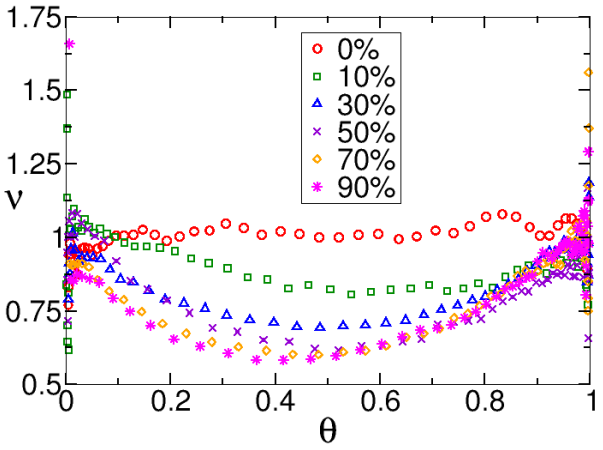

FIG. 10: (Color Online) Preexponential factor (ν) as a function of coverage (θ) for all regimes of interaction strength, indicated in the legend as a percentage of the surface binding strength $E_b = 100$.

kinetics. As a result, due to the added energy contributions when interactions are present, the sites become energetically heterogeneous. To illustrate this point, Fig. 8 shows $P(z_o)$ for one interaction energy at several values of the coverage, which demonstrates how the distribution of the occupation coordination becomes wider at coverages away from complete and zero coverage.

B. Preexponential Factor

The preexponential factor is obtained by computing the ratio of two desorption rates. One is the direct numerical derivative with respect to time $\dot{\theta}$ (symbols in Fig. 9) of the coverage decrease data (from Fig. 6(a)). This yields the typical TPD spectra. The second is the analytically calculated rate for each interaction regime (solid lines in Fig. 9), using Eq. 3 with the numerical desorption decrease data, and average energy per site (from Fig. 7) with $\nu = 1$. A comparsion between the two shows a difference that increases with interaction strength, indicating some degree of variation in the prefactor, *and some level of compensation between E_a and ν*. The extracted preexponential factor is plotted as function of coverage in Fig. 10 where, in the non-interacting regime, ν remains constant at unity (the observed fluctuations are due to the numerical derivatives) while, for $\epsilon > 0$, ν exhibits a systematic deviation from the non-interacting value as the interaction strength increases. In this sense $\nu(\epsilon = 0)$ is the bare desorption rate that is renormalized in the presence of interactions. A thermodynamic point of view posits that the changes in ν can be attributed to changes in the entropy [10, 33, 45]. This view is somewhat contained within the Erying-Polanyi equation [4, 46, 47]

$$k = \kappa \frac{k_B T}{h} e^{\frac{\Delta S}{k_B}} e^{\frac{-\Delta H}{k_B T}}, \tag{7}$$

where h is Planck's constant, E_a is associated with the enthalpy of activation ΔH, and ν has a frequency component κ, a temperature dependence, and an entropy component ΔS [10]. It follows that, for the non-interacting case ($\epsilon = 0$), the frequency component of ν is unchanged due to the fact that desorption and diffusion events are unaffected by the presence of nearest neighbors, as seen in Fig. 10, whereas for the entropy component, ν always starts and ends at (or close to) 1. At intermediate times/temperatures, the number of available microstates increases due to more possible distributions of particles on the surface. The initial phase of desorption occurs through eating away of the large, percolating, connected clusters of occupied sites. Yet, in the non-interacting regime, there is a lack of correlation as to which sites become unoccupied. As ϵ increases, site occupation is correlated over longer timescales since desorption and diffusion events are slowed down, resulting in a decrease in the frequency of events, as well as in the configurational entropy, an indicator of the compensation effect [33]. These enhanced correlations can be quantified through the time autocorrelation function for site occupancy, $C_j =< \sigma_j(t+\tau)\sigma_j(t) >$, where σ is the site occupation number and takes on the values 0 or 1, and τ is the time lag over which correlations are measured. These results, shown in Fig. 11(a), demonstrate that correlations in site occupation become greatly enhanced as

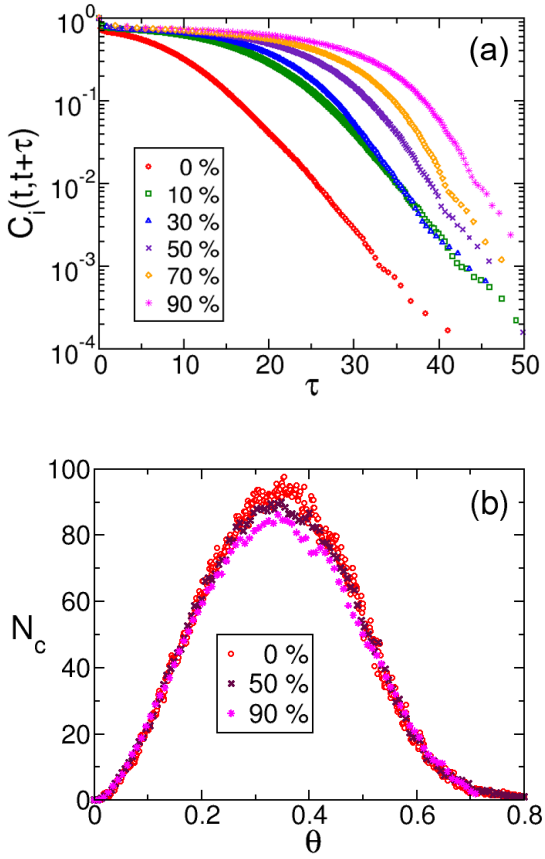

FIG. 11: (Color Online) Correlation and cluster analyses. Fig. (a): site time autocorrelation function C_j (see text for definition), for various interaction strengths, indicated in the legend as a percentage of the surface binding energy. Simulation times were chosen to span the desorption processes for the different energies. Fig. (b): number of distinct clusters (N_c) as a function of coverage for zero, intermediate, and large interaction strengths.

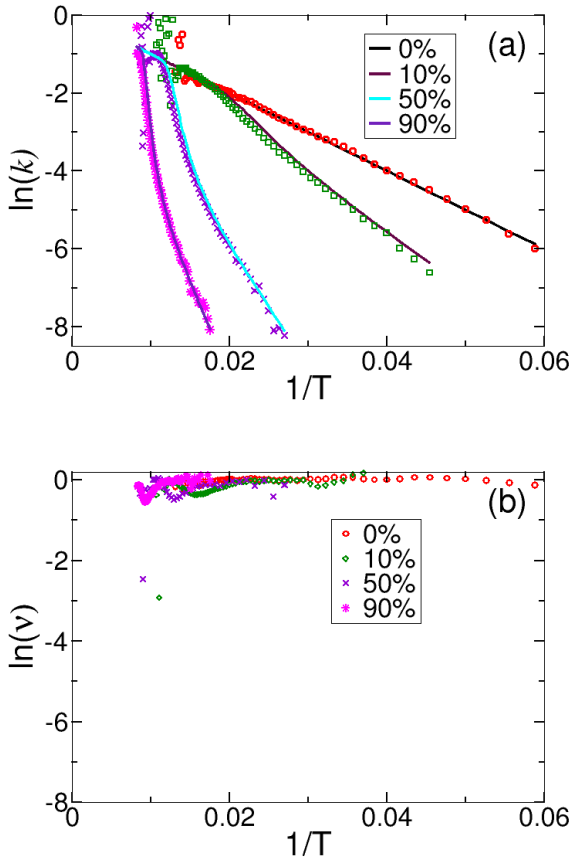

FIG. 12: (Color Online) Fig. (a): Arrhenius plots calculated as $\ln k = -E_a/k_BT$, with $\nu = 1$ (solid lines), superimposed with the Arrhenius plots from Fig. 6 for selected regimes of interaction strength, indicated in the legend as a percentage of the surface binding strength. Fig. (b): Contribution of the preexponential factor to the same Arrhenius plots, calculated as $\ln k = \ln \nu$.

ϵ increases. As desorption proceeds, the occupied lattice starts to break up into connected (smaller) island clusters of occupied sites, as has been observed experimentally [48]. The number of clusters reaches a maximum at a coverage value where both depend on interaction strength (see Fig. 11(b)).

We can interpret these features as follows: for a given value of the coverage, systems with stronger interactions are likely to exist in larger but fewer clusters, due to enhanced site correlations that persist for longer times/temperatures. If the number of clusters decreases, the entropy is expected to decrease, which is reflected in the value of ν in Fig. 10. The data in Fig. 11 show that the coverage at which the difference in the number of clusters is largest coincides with the greatest difference in the ν values in Fig. 10. And, although the numerical difference in the number of clusters of Fig. 11 appears insignificant at first sight (only about 10% difference), it becomes significantly magnified when evaluating the entropy through counting the number of accessible microstates.

C. Kinetic Compensation Effect

The separate contributions of E_a and $\ln \nu$ to the Arrhenius plots are shown in Fig. 12 for various regimes of interaction strength. Fig. 12(a) shows two sets of superimposed Arrhenius plots. The symbols represent the plots calculated directly from the desorption data as $\ln \frac{\dot{\theta}}{\theta}$. The solid lines represent the Arrhenius plots calculated by taking into account only the contribution from the activation energy (and ν is set to 1), as $\ln k = \frac{-E_a}{k_BT}$, with the numerical data for E_a. The curvatures of these plots remain almost unchanged, indicating that the relative

contribution from $\ln\nu$ is rather small. Fig. 12(b) shows this contribution as $\ln\nu$ vs. $^1/_T$. It can be seen that $\ln\nu$ remains approximately constant and relatively close to 1 throughout the process. While this could be interpreted as a lack of compensation, the results in Fig. 9, as well as those in Fig. 10, show that the prefactor does exhibit variations that are consistent with a decrease in configurational entropy as a consequence of stronger binding strength [33], therefore supporting the occurrence of a *partial* compensation effect between E_a and $\ln\nu$. This does not seem to change significantly with increasing ϵ.

From these results we observe that, for this system, caution should be exercised when attempting to develop analytical expressions to describe the behavior of the parameters in a manner that is consistent with their variations occuring in the same direction and with almost the same magnitudes. This may be the case in other systems.

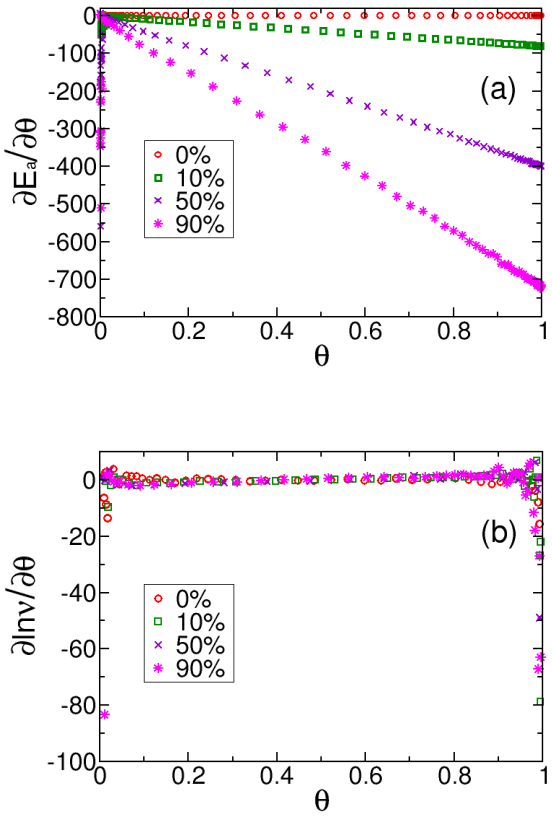

FIG. 13: (Color Online) Second order, coverage dependent terms appearing in the parentheses of Eq. 8 for selected regimes of interaction strength, indicated in the legend as a percentage of the surface binding strength. The derivatives of E_a (Fig. (a)) and $\ln\nu$ (Fig. (b)), with respect to coverage θ are expected to add to zero as a special manifestation of the compensation effect.

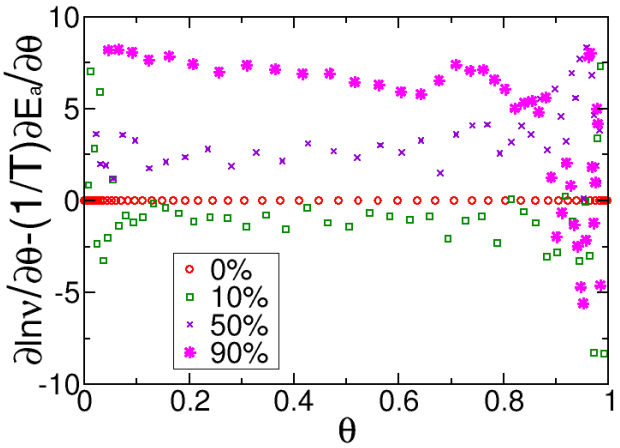

FIG. 14: (Color Online) Calculated second order terms in parentheses in Eq. 8 for some regimes of interaction strength, indicated in the legend as a percentage of the surface binding strength $E_b = 100$. The second order terms only add to zero in the non-interacting regime.

D. False kinetic compensation effects in Thermal Desorption

A theory which predicts the variations in E_a and $\ln\nu$ to occur in a mutually offsetting manner was previously explained by Miller et al. [1] and by Nieskens et al. [25], as a possible cause for a false KCE. This theory states that, in the presence of lateral interactions, the Arrhenius parameters become coverage dependent. Then, considering all explicit dependencies, the slope of the Arrhenius plot, $\frac{d\ln k}{d(1/T)}$, becomes [1, 25]

$$-\frac{E_a(\theta)}{k_B} + \frac{d\theta}{d\,(1/T)}\left(\frac{\partial \ln\nu(\theta)}{\partial\theta} - \frac{1}{k_B T}\frac{\partial E_a(\theta)}{\partial\theta}\right), \quad (8)$$

where the second order terms (in parentheses) yield a non-constant slope, and can only be ignored if: (1) the parameters are constant, (2) measurements are made over a region where the change in the coverage is vanishingly small $\left(\frac{d\theta}{d(1/T)} \sim 0\right)$, or (3) the terms sum to zero, i.e. $\frac{\partial\ln\nu(\theta)}{\partial\theta} = \frac{1}{k_B T}\frac{\partial E_a(\theta)}{\partial\theta}$, as a special manifestation of the compensation effect, and the solution to the resultant differential equation reduces to Eq. 2 [1, 25].

The derivatives with respect to coverage were calculated using the numerical data, and the results are shown in Fig. 13. In Fig. 13(a), the derivative of E_a exhibits much larger variations than $\ln\nu$ (Fig. 13(b)). When the terms are added, according to Eq. 8, the result is only zero in the non-interacting case, as expected. Otherwise, it yields a non-zero, finite contribution, shown in Fig. 14. This is the case even when the factor $^1/_{k_B T}$ attenuates variations in $\frac{\partial E_a(\theta)}{\partial\theta}$. The increasing curvature of the Ar-

rhenius plots in Fig. 6(b) should be the first visible indicator that the second order terms do not add to zero. When this is ignored, a straight line is imposed upon the data, which can lead to a false KCE [1, 25].

E. Isokinetic relation (IKR)

The Arrhenius plots in Fig. 6(b) exhibit a tendency to converge towards the region of high temperature and low coverage, but they do not cross at a single value of T_c, such as those in the idealized set shown in Fig. 1. However, the interacting curves cross the non-interacting one, or an extrapolation of it, at different points. The values of T at these crossings were visually estimated, as indicated by the vertical lines in Fig. 15, and the obtained values are shown in Table I, where they are referred to as compensation temperatures. The numerically calculated values of E_a, ν, and $\ln k$ at the crossing temperatures are also displayed in Table I.

TABLE I: Numerical values of E_a and ν at approximate compensation temperatures. The numerical values of the energies of activation approach the binding energy of the surface, and the values of ν are close to 1, indicating a transition to a non-interacting regime at the corresponding T_c.

ϵ	T_c	E_a	ν	$\ln k$
10%	60	-100.35	1.01	-1.67
30%	78	-100.12	0.93	-1.36
50%	89	-100.64	1.0	-1.13
70%	104	-100.32	0.91	-1.06
90%	118	-100.24	0.88	-0.98

When an IKR is observed, the rates are expected to acquire similar values and become independent of external perturbing parameters at T_c [5] and, if all the rates have the same equilibrium value, it is said that they have reached *isokinetic equilibrium*. The values of k in Table I are not exactly equal. Nevertheless, they become independent of external parameters since the calculated values of E_a and ν show that, at the crossing temperatures, the rates are governed only by the parameters of the surface. This makes physical sense because this occurs in the region of low coverage and high temperature but, perhaps more importantly, the convergence does not seem to occur due to a compensation between E_a and ν.

The discrepancy in the crossing temperatures for each Arrhenius plot can be attributed to the 10% difference between regimes of interaction strength, and it would be of interest to observe what happens if a different parameter is varied while keeping the interaction strength the same.

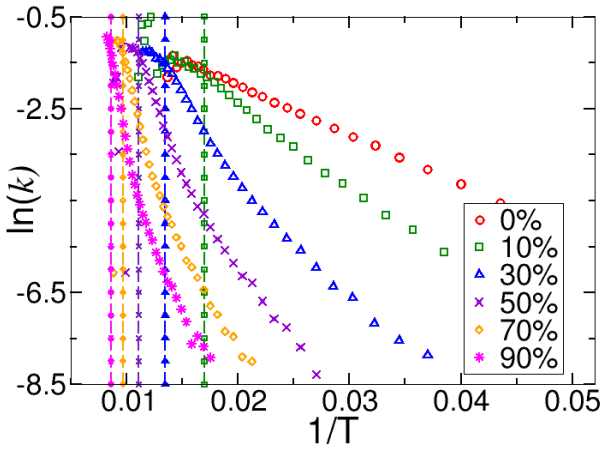

FIG. 15: (Color Online) Estimated compensation temperatures for all Arrhenius plots in Fig. 6(b), indicated by the vertical lines in the same color as the corresponding curve. The interaction strength is indicated in the legend as a percentage of the surface binding energy $E_b = 100$.

F. Weak Adsorbate Interactions

Compensation effects continue to be reported in many different fields of science [2, 5], therefore this discussion would not be complete without addressing a regime of interaction strength in which a KCE and an IKR, as currently defined, would be observed. In thermal desorption this corresponds to adsorbate-adsorbate interaction strengths that fall within the range $\epsilon \leq 10\%$ of the binding energy of a planar, energetically homogeneous surface, such as the desorption of Xe from graphite [49]. The numerical results in this regime are plotted in Fig. 16.

The Arrhenius parameters were extracted through a linear fit, and are displayed in Table II, along with selected results for stronger interaction regimes, obtained through the same method, for comparison. The numerically calculated values of $E_{a,max}$ and $< \nu >$ are also shown. For weakly interacting adsorbates, the fit provides reasonably accurate estimates while, at stronger values of ϵ, deviations grow dramatically. These results present a stark contrast with strong coverage dependent preexponential factors which can be obtained in the regime of strong interactions [14, 19, 20, 50, 51], and which have been identified as an indicator of false compensation effects in thermal desorption [25], mainly due to forced linearization [14, 44]. Since the Arrhenius plots in Fig. 16 cross, the compensation temperature was estimated (rightmost dashed line in the figure) to be $T_c = 59.17$.

The corresponding Constable plot for $(E_{a,i}, \ln \nu_i)$ data pairs in the interaction range $1\% - 9\%$ is displayed in Fig. 17, with a linear correlation coefficient of 0.99998.

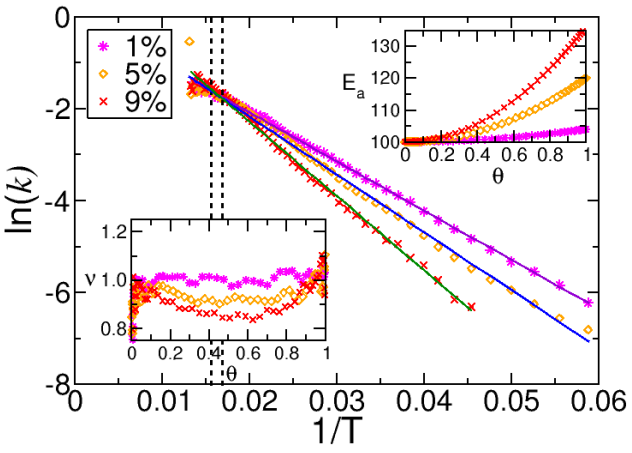

FIG. 16: (Color Online) Arrhenius plots for interaction strengths $\epsilon = 1\%$, 5%, and 9% of the surface binding energy. The symbols are the simulation data, and the solid lines are the best linear fits to the Arrhenius plots. The vertical dashed lines indicate a visually estimated compensation temperature $T_c = 59$ (left line), and $T_c = 65$ (right line), obtained from the slope of the Constable plot in Fig. 17. The insets show E_a (top) and ν (bottom) as function of coverage (θ).

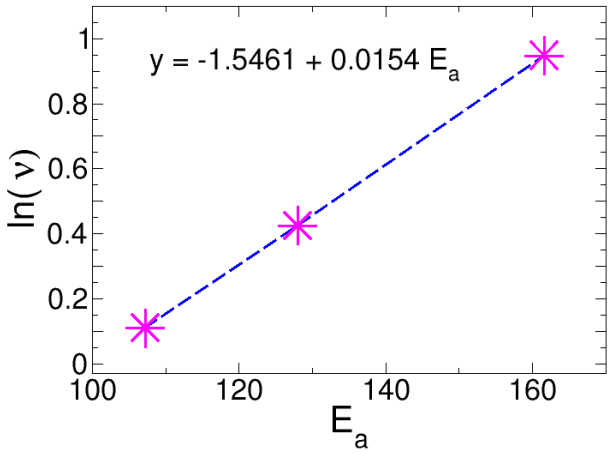

FIG. 17: (Color Online) Constable plot using fitted parameters E_a and $\ln \nu$ for interaction strength regimes of 1%, 5%, and 9% of the surface binding energy. A linear fit of Eq. 2 to this plot (dashed line) yields $\beta = 0.0154$, which corresponds to temperature $T_c = 68.94$ and $\alpha = -1.5461$. Note that the x axis starts at 100.

TABLE II: Arrhenius parameters, E_a and ν, obtained through linear fits to the Arrhenius plots. The results are compared to the numerically calculated values from the simulations. The percentage error increases with interaction strength.

ϵ	E_a max.	E_a linear fit	$<\nu>$ calculated	ν linear fit
0%	100	102	0.99	1.0
1%	104	107	1.02	1.12
5%	120	125	0.96	1.41
9%	145	161	0.931	2.58
10%	140	167	0.93	2.4
30%	220	292	0.89	8.18
90%	460	785	0.89	121.94

TABLE III: Numerical values of E_a, ν, and $\ln k$, at $T = 59$ and $T_c = 65$, obtained from a linear fit to the Constable plot in Fig. 17 using Eq. 2. The numerical values of the rates, and the numerical values of E_a, indicate a transition to the non-interacting regime, where the rates are governed solely by the bare parameters of the surface.

ϵ	T_c	E_a at T_c	ν at T_c	$\ln k$ at T_c
1%	59	-100.00	0.97	-1.67
5%	59	-100.07	0.93	-1.69
9%	59	-100.33	1.05	-1.65
1%	65	-100.00	0.99	-1.55
5%	65	-100.00	0.96	-1.54
9%	65	-100.03	1.07	-1.47

This indicates the observation of a KCE according to traditional criteria. However, the insets in Fig. 16 show that the parameters vary in the same manner as they did in stronger interaction regimes, supporting the occurrence of a partial compensation effect instead of a complete one. The slope of the line in Fig. 17 yields $T_c = 64.94$, indicated by the leftmost dashed line in Fig. 16. This is higher than the previous estimate of $T_c = 59$. The numerically calculated values of E_a and ν at both $T = 59.17 \approx 59$ and $T = 64.94 \approx 65$ are displayed in Table III. The data show that, in both instances, the effects of lateral interactions tend to become negligible at T_c, and the rates acquire close values.

The intercept of the Constable plot is $\alpha = \ln k_c = -1.5461 \approx -1.55$, this is close to the rates at $T = 65$. The rates do not have the exact same value, but the results show a transition to the non-interacting regime.

The KCE and IKR are generally attributed to weak molecular interactions [24], and the numerical results in this regime predict an IKR and a KCE in the form of Eq. 2, with $\alpha = -1.5461$ and $\beta = 0.0154$. However, strict adherence to these criteria exclude the occurrence of compensation effects in stronger interaction regimes. A decrease in configurational entropy due to molecular interactions should be expected, and not only in the case of weak association [34]. The numerical results presented here show a compensation effect occurring even in the case of curved Arrhenius plots, at stronger interaction regimes. Nevertheless, the linear fit in this case becomes

inadequate. It should also be noted that the implication of a complete mutual offsetting is that the effects of interactions are not perceivable, and this would exclude the curved Arrhenius plots.

IV. CONCLUSIONS

Our results support the existence of a behavior that yields a compensation effect between E_a and ν. However, the observed changes in the preexponential factor *are not large enough to completely offset the significant variations in the activation energy,* E_a, which arise due to strong coverage dependence. This produces a net *partial* compensation between E_a and $\ln \nu$ for all regimes of interaction strength presented in this study. This is true even in the case where a strong linear correlation, which satisfied Eq. 2 for constant α and β, was observed (regime of weak interactions). Therefore it is reasonable to conclude that Eq. 2 represents the functional dependence of the *apparent* (and *fixed*) Arrhenius parameters for systems which exhibit an Arrhenius type behavior as E_a is varied through an external experimental parameter. However, *it does not predict their transient variations*. Not only do the parameters not completely compensate each other, but this prediction precludes the consideration of these effects in systems which deviate from straight Arrhenius plots. This is counterintuitive, since a stronger binding strength should be associated with a more pronounced decrease in the configurational entropy, and therefore with an increased level of compensation between E_a and $\ln \nu$, compared to the regime of weak interactions. Partial compensation has been previously considered [2, 4], but this notion is not as widespread as that of a complete KCE.

We observed an IKR in the regime of weak interactions. At T_c the rates became similar due to the system transitioning to a regime where the effects of lateral interactions become negligible, thus the rates become independent of external perturbations. A single crossing temperature was not observed for the other stronger interaction regimes presented in this study, this is likely due to the 10% difference between them. However, those interacting curves approached the non-interacting one at different temperatures. This also occurred in the region of low coverage and high T. The numerically calculated values of E_a and ν at those temperatures indicate that this is also due to the transition to the non-interacting regime.

The behavior we observed may help clarify compensation effects and isokinetic relations observed in other systems. A better understanding of this phenomenon can help achieve controlled activated events and provide a means to accurately parameterize many biological, chemical, and physical processes that share common features in their compensation effects.

ACKNOWLEDGMENTS

N. Zuniga-Hansen and M. M. Calbi acknowledge support provided by the National Science Foundation through grant CBET-1064384.

The authors would also like to thank Professor Phillip Sprunger for valuable discussions.

[1] J. B. Miller, H. R. Siddiqui, S. M. Gates, J. N. Russell Jr., J. T. Yates, J. C. Tully and M. J. Cardillo, J. Chem. Phys. **87**, 6725 (1987).
[2] L. Liu and Q.-X. Guo, Chem. Rev. **101**, 673 (2001).
[3] B. V. L'vov and A. K. Galwey, International Reviews in Physical Chemistry **32**, 515 (2013).
[4] A. Yelon, E. Sacher and W. Linert, Phys. Chem. Chem. Phys. **14**, 8232 (2012).
[5] K. F. Freed, J. Phys. Chem. B **115**, 1689 (2011).
[6] H. J. Kreuzer and N. H. March, Theor. Chim. Acta **74**, 339 (1988).
[7] P. J. Barrie, Phys. Chem. Chem. Phys. **14**, 318 (2012).
[8] F. Constable, Proc. R. Soc. London **A108**, 355 (1923).
[9] P. J. Barrie, Phys. Chem. Chem. Phys. **14**, 327 (2012).
[10] G. Gottstein and L.S. Shvindlerman, Interface Sci. **6**, 265 (1998).
[11] R. K. Agrawal, J Therm Anal Calorim **31**, 73 (1986).
[12] J. F. Douglas, J. Dudowicz and K. F. Freed, Phys. Rev. Lett. **103**, 135701 (2009).
[13] W. Linert, Chem. Soc. Rev. **18**, 477 (1989).
[14] V. P. Zhdanov, Surf. Sci. Lett. **12**, L662 (1991).
[15] P. J. Barrie, C. A. Pittas, M. J. Mitchell and D. I. Wilson, Proceedings of International Conference on Heat Exchanger Fouling and Cleaning (2011).
[16] K. A. Fichthorn and W. H. Weinberg, Langmuir **7**, 2539 (1991).
[17] K. A. Fichthorn and P. G. Balan, J. Chem. Phys. **101**, 20028 (1994).
[18] S. Payne and H. J. Kreuzer, Surf. Sci. **404**, 222 (1989).
[19] V. P. Zhdanov, Surf. Sci. **209**, 523 (1989).
[20] V. P. Zhdanov, Surf. Sci. **111**, L662 (1981).
[21] H. C. Kang, T. A. Jachimowski and W. H. Weinberg, J. Chem. Phys. **93**, 1418 (1990).
[22] P. J. Estrup, E. F. Greene, M. J. Cardillo and J. C. Tully, J. Phys. Chem. **90**, 4099 (1986).
[23] E. Tomkova and I. Stara, Vacuum **50**, 227 (1998).
[24] J. D. Dunitz, Chemistry & Biology **2**, 709 (1995).
[25] D. L. S. Nieskens, A. P. van Bavel ans J. W. Niemantsverdriet, Surf. Sci. **546**, 159 (2003).
[26] A. Cornish-Bowden, J. Biosci. **27**, 121 (2002).
[27] N. Koga and J. Šesták, Thermochim. Acta **182**, 201 (1991).
[28] I. Banik, R. Banik, J. Lukoviova and G. Pavlendova, Chalcogenide Lett. **10**, 455 (2013).
[29] J. C. Dyre, J. Phys. C: Solid State Phys. **19**, 5655 (1986).
[30] D. S. Rawat , T. Furuhashi and A. D. Migone, Langmuir **25**, 973 (2009).
[31] V. Krungleviciute, C. A. Ziegler, S. R. Banjara, M. Yu-

dasaka, S. Iijima and A. D. Migone, Langmuir **29**, 9388 (2013).
[32] Y. C. Kim and J. Mittal, Phys. Rev. Lett. **110**, 208102 (2013).
[33] C. Piguet, Dalton Trans. **5**, 8059 (2014).
[34] D. M. Ford, J. Am. Chem. Soc. **127**, 16167 (2005).
[35] A. F. Voter, in *Radiation Effects in Solids*, edited by K. E. Sickafus, E. A. Kotomin, and B. Uberuaga (Springer, Dordrecht. The Netherlands, 2007), vol. 235 of *NATO Science Series*, chap. Introduction to the Kinetic Monte Carlo Method, pp. 1–23.
[36] A. M. Hansen and J. O. Leckie, Advances in Water Resources **21**, 523 (1998).
[37] P. Coufalik, O. Zverina and J. Komarek, Chemical Papers **68**, 427 (2014).
[38] M. T. Smith, F. Berruti, and A. K. Mehrotra, Ind. Eng. Chem. Res. **40**, 5421 (2001).
[39] R. P. Redhead, Vacuum **12**, 203 (1962).
[40] J. T. Burde, N. Zuniga-Hansen, C. L. Park and M. M. Calbi, J. Phys. Chem. C **113**, 16945 (2009).
[41] N. Zuniga-Hansen and M. M. Calbi, J. Phys. Chem. C **116**, 5025 (2012).
[42] J. Burde and M. M. Calbi, J. Phys. Chem. Letters **1**, 808 (2010).
[43] V. H.C. Silva, V. Aquilanti, H. C. B. de Oliveira and K. C. Mundim, Chem. Phys. Lett. **590**, 201 (2013).
[44] S.H. Payne, A. Wierzbicki and H.J. Kreuzer, Surf. Sci. **242**, 291 (1993).
[45] K. Sharp, Protein Science **10**, 661 (2001).
[46] H. Erying, J. Chem. Phys. **3**, 107 (1935).
[47] H. Erying, Chemical Reviews **17**, 65 (1935).
[48] S. Gunther, T.O. Mentes, M.A. Niño, A. Locatelli, S. Bocklein and J. Wintterlin, Nat. Commun. **5**, 3853 (2014).
[49] H. Ulbricht, J. Kriebel, G. Moos and T. Hertel, Chem. Phys. Lett. **363**, 252 (2002).
[50] E.G. Seebauer, A.C.F. Kong and L.D. Schmidt, Surf. Sci. **193**, 417 (1988).
[51] H. E. H. Pfnur, P. Feulner and D. Menzel, Chem. Phys. Lett. **59**, 481 (1978).